



Deposited via The University of Sheffield.

White Rose Research Online URL for this paper:

<https://eprints.whiterose.ac.uk/id/eprint/215382/>

Version: Accepted Version

Article:

Peng, Z., Stovin, V. and Guymer, I. (2024) Radial mixing in steady and accelerating pipe flows. *ASCE Journal of Hydraulic Engineering*, 150 (6). ISSN: 0733-9429

<https://doi.org/10.1061/JHEND8.HYENG-14071>

© 2024 The Author(s). Except as otherwise noted, this author-accepted version of a journal article published in *Journal of Hydraulic Engineering* is made available via the University of Sheffield Research Publications and Copyright Policy under the terms of the Creative Commons Attribution 4.0 International License (CC-BY 4.0), which permits unrestricted use, distribution and reproduction in any medium, provided the original work is properly cited. To view a copy of this licence, visit <http://creativecommons.org/licenses/by/4.0/>

Reuse

This article is distributed under the terms of the Creative Commons Attribution (CC BY) licence. This licence allows you to distribute, remix, tweak, and build upon the work, even commercially, as long as you credit the authors for the original work. More information and the full terms of the licence here: <https://creativecommons.org/licenses/>

Takedown

If you consider content in White Rose Research Online to be in breach of UK law, please notify us by emailing eprints@whiterose.ac.uk including the URL of the record and the reason for the withdrawal request.

Radial Mixing in Steady and Accelerating Pipe Flows

Zhangjie Peng¹, Virginia Stovin² and Ian Guymer³

¹Research Associate, Department of Civil and Structural Engineering, The University of Sheffield, Mappin Street, Sheffield, S1 3JD, United Kingdom. Email: zhangjie.peng@sheffield.ac.uk

²Professor of Green Infrastructure for Stormwater Management, Department of Civil and Structural Engineering, The University of Sheffield, Mappin Street, Sheffield, S1 3JD, United Kingdom. Email: v.stovin@sheffield.ac.uk

³Professor of Civil Engineering, Department of Civil and Structural Engineering, The University of Sheffield, Mappin Street, Sheffield, S1 3JD, United Kingdom. Email: i.guymer@sheffield.ac.uk

ABSTRACT

Understanding solute transport in pipe flows is essential for ensuring consistent water quality throughout the entire drinking water supply network. This study utilised four Planar Laser-Induced Fluorescence (PLIF) units for the first time to quantify the cross-sectional concentration distribution resulting from a single pulse of tracer injected at an upstream location under both steady and accelerating flow conditions. In comparison with conventional fluorometers, PLIF provides a better measure of the cross-sectional mean concentrations, because it allows the cross-sectional distribution of the tracer to be quantified. Under steady turbulent flow conditions, the tracer was cross-sectionally well-mixed, and the concentration uniformity increased with increasing Reynolds number. In laminar flows, as a result of minimal radial mixing, the tracer exhibited a spatial distribution created by the longitudinal differential advection, transforming from a central core to an annulus, which expanded towards the pipe boundary. Under accelerating flows, the temporal concentration profiles displayed two peaks and the tracer close to the source was not cross-sectionally well-mixed. With increasing discharge, the tracer became cross-

24 sectionally well-mixed while retaining the two peak profiles. These results have implications for
25 water quality modelling in unsteady conditions, especially in domestic plumbing, when boundary
26 and biofilm interactions control important processes.

27 Keywords: Solute Transport; Steady; Unsteady; Pipe Flow; Concentration Distribution.

28 INTRODUCTION

29 Understanding solute transport in drinking water distribution networks is key to maintaining
30 consistent water quality throughout the networks. The ability to accurately model the peak
31 concentration and longitudinal spread of disinfectants or accidentally introduced contaminants in the
32 network is critical for protecting public health (Piazza *et al.*, 2020, Lee *et al.*, 2023). In main drinking
33 water distribution networks, the flow condition is typically considered to be steady turbulent flow, in
34 which advection outweighs the impact of longitudinal dispersion. Many water quality models for
35 distribution networks assume turbulent flow conditions, and only model bulk advection, neglecting
36 longitudinal dispersion (Rossman, 2000; Romero-Gomez and Choi, 2011). However, in peripheral
37 regions, where water leaves the main network and enters the customers' consumption points, laminar
38 and transitional flow conditions exist in the pipe (Buchberger *et al.*, 2003; Shang *et al.*, 2023). In
39 premises plumbing systems, flow conditions tend to be laminar for much longer periods, increasing
40 water quality concerns due to the risks associated with human exposure to contaminants (Lee *et al.*,
41 2023).

42 In a distribution network, flow is not steady. Various factors, such as pump stoppage, sudden changes
43 in local intermittent demand, or the opening and closing of valves, can lead to periods of unsteady
44 discharge in all parts of the network (Hart *et al.*, 2021; LeChevallier *et al.*, 2003). Experimental studies
45 on unsteady flows have focused on measuring temporal local mean radial velocity profiles at a single
46 location (Greenblatt and Moss, 2004; He and Jackson, 2000; Kurokawa and Morikawa, 1986).
47 However, these measurements lack the short-term, temporal turbulent velocity fluctuations across

48 pipe radius during the unsteady flows that are needed to quantify the local radial mixing
49 characteristics. Therefore, there is a pressing need for an understanding and improved modelling of
50 how contaminants travel and spread in unsteady flow scenarios (Burkhardt *et al.*, 2020; Shang *et al.*,
51 2023, Lee *et al.*, 2023).

52 Solute tracers used to determine longitudinal dispersion are required to be easy to detect and have
53 similar physical properties to water. Fluorescent tracers serve this purpose well as they are mostly
54 conservative, have a low limit of detection, and are used extensively in various applications (Swarnkar
55 *et al.*, 2022; Wilson *et al.*, 1986). Fluorometers are devices to measure fluorescent tracer
56 concentrations. The Turner Designs Series 10 fluorometer (Turner Designs, San Jose, California) is
57 designed to take static cuvette samples and dynamic flow-through measurements. Hart *et al.* (2016,
58 2021) employed a number of these fluorometers, with a 24 mm internal diameter perspex pipe
59 passing through, for nonintrusive concentration measurements under different steady and unsteady
60 flow conditions. These fluorometers output a single concentration value at each time step, and in their
61 analysis, the authors treated this value as the cross-sectional area mean concentration. However, in
62 laminar flows, the tracer is usually not perfectly cross-sectionally well-mixed, and such measurements
63 may not accurately represent the cross-sectional area mean concentrations at these conditions.

64 Laser Induced Fluorescence (LIF) is a nonintrusive measurement technique based on optical principles
65 used for qualitative and quantitative descriptions of flow and mixing phenomena. van Cruyningen *et al.*
66 (1990) demonstrated that it was possible to use laser light-sheets as an illumination source for
67 fluorescent dye concentration measurements. Harry *et al.* (1996) developed an in-situ concentration
68 measurement technique to investigate vertical mixing processes in a laboratory representation of the
69 coastal zone. A typical LIF system consists of an illumination source (laser), fluorescent compounds,
70 image acquisition devices (camera) and illumination optics (Crimaldi, 2008). With the aid of optics, a
71 light sheet can be generated to illuminate a plane area. Planar Laser-Induced Fluorescence (PLIF)
72 offers the opportunity to measure 2D (cross-sectional) concentration distributions, which can also be
73 used to determine an accurate pipe cross-sectional mean concentration. To date, no study has

74 attempted to employ PLIF to measure 2D concentration distributions at multiple locations for pipe
75 flows.

76 When a solute or contaminant is introduced into pipe flow, it disperses in all directions. Longitudinal
77 dispersion is caused by the combined effects of cross-sectional differential advection and radial
78 diffusion. For a pulse of contaminant, this changes the area mean temporal solute concentration
79 profile as it travels along the flow direction, reducing the peak concentration and increasing the
80 spread. Studies on pipe mixing have focused on quantifying longitudinal dispersion under different
81 steady flow conditions using measured tracer temporal cross-sectional mean concentration profiles
82 at different downstream locations (Fowler and Brown, 1943; Taylor, 1954; Flint and Eisenklam, 1969;
83 Keyes, 1955; Hart *et al.*, 2016; Piazza *et al.*, 2020). In these studies, the tracer concentration was
84 measured either at the pipe wall, through tapping points, at the discharge point or non-invasively by
85 fluorometers at different downstream locations along the pipe. These measurements lead to a 1D
86 concentration measurement, often assumed to be the cross-sectional mean value. No study has
87 directly measured 2D spatial distributions over the pipe cross-section.

88 Pipe flows can be categorised into laminar, transitional, and turbulent flow, each exhibiting distinct
89 mixing characteristics. Laminar flow is characterised by streamline motion, where the only velocity
90 component is longitudinal, and the radial exchange is due to molecular diffusion. This generates high
91 values of longitudinal dispersion, D_x (m^2/s), with the dimensionless longitudinal dispersion coefficient,
92 $D_x^* = D_x/\bar{u}d$, of around 20 at $\text{Re} = 2,000$, where \bar{u} = cross-sectional mean velocity and d = pipe
93 internal diameter. In turbulent flow, rapid local velocity fluctuations promote radial mixing, leading to
94 lower longitudinal dispersion, with D_x^* of around 0.4 at $\text{Re} = 50,000$ (Hart *et al.*, 2016). Transitional
95 flow represents a condition where either laminar or turbulent flow can occur (Mathieu and Scott,
96 2000).

97 Hart *et al.* (2021) investigated longitudinal dispersion in unsteady pipe flows. Both accelerating and
98 decelerating flow cases were studied, within the turbulent flow range and between laminar and

99 turbulent flow conditions. In most cases, the 1D concentration measured by the fluorometers revealed
100 single peaked distributions at each location. The exception was during acceleration from laminar to
101 turbulent flow conditions when a previously unreported disaggregation of the single 1D tracer cloud
102 was observed. This is illustrated in Fig. 1, where the upstream temporal concentration profile,
103 recorded during flows with $Re \approx 3,500$, exhibited a single peak distribution, following the expected
104 Gaussian form of distribution. Once this single pulse of tracer experienced accelerating flows, upto Re
105 $\approx 8,000$, it was shown to disaggregate into multiple pulses over the following ~ 2 m length of pipe.

106 *Insert Fig. 1*

107 The mechanism responsible for creating the observed disaggregation was not identified, as
108 measurements were limited by the 1D area mean concentrations and the lack of hydrodynamic
109 measurements. Hence, as a first step to understand the physical processes, this paper presents novel
110 measurements to explore the temporal variation of cross-sectional tracer distribution (tracer
111 uniformity) in pipe flows accelerating from laminar to turbulent conditions. The objectives of this
112 study are to:

- 113 1. Quantify the limitations of using 1D fluorometers for determining area mean concentration;
- 114 2. Visualise pipe 2D spatial and temporal tracer concentration distributions under steady and
115 accelerating flows;
- 116 3. Quantify the degree of tracer uniformity over the pipe cross section during these conditions.

117 **MATERIALS AND METHODS**

118 **Experimental Rig**

119 Experiments were conducted on a section of 13 m long, 24 mm internal diameter perspex pipe (Fig.
120 2(a)). This test section was connected to a recirculating system, with water from a ground-level sump
121 (3 m^3) pumped to a 1 m^3 header tank 10 m above, before entering the test section. To maintain a
122 constant water head, an overflow pipe was installed on the upper tank. A perspex plate (inlet in Fig.

123 2(a)) with an opening of 4.75 mm was placed before the test section to reduce the flow rate within
124 the test section. Flow control was achieved with a digital butterfly valve (Series J3C, J+J Deutschland
125 GmbH, Germany) located at the end of the test section.

126 During the experiment, a fluorescent tracer, Rhodamine 6G, was injected into the flow from the pipe
127 wall using a pressurised vessel equipped with a solenoid valve. The injection point was 2.043 m
128 downstream from the start of the test section, a length considered sufficient for flow to be fully
129 developed. The pressure vessel maintained a constant pressure of 2.0 bar, and the computer-
130 controlled solenoid valve ensured consistent injected tracer volume and timing. The injection pressure
131 used in this study is to ensure a cross-sectional well-mixed condition at the injection point and
132 minimise the influence of injection on the downstream concentration distributions. Fig. 2(b) visualises
133 the dye distribution near the injection location after the injection using a red food dye, the dye was
134 cross-sectionally well-mixed at the first few centimetres downstream of the injection location.

135 The discharge from the pipe was determined from a calibrated differential pressure transducer
136 (PD33X, KELLER, Switzerland) across a 7 mm diameter orifice. The relationship between the
137 differential pressure transducer output, digital butterfly valve opening and the discharge was
138 calibrated using volumetric measurements of discharge. Two tapping points were made on the pipe,
139 11.779 m apart, for measuring the pipe head loss with a calibrated differential pressure transducer
140 (PXM409-025HDWUI, OMEGA Engineering, USA).

141 To ensure that the most of tracer passed all the measurement locations during the accelerating flow
142 zone, instruments were placed within 6 m downstream of the injection location. Four Turner Designs
143 Series 10 fluorometers, F1 to F4 (Turner Designs, San Jose, USA) were placed downstream of the
144 injection point to non-intrusively measure the temporal concentration profiles. The pipe passed
145 through the fluorometers, and all the outside sections were covered with black sheets to prevent the
146 interference of external light. Four Planar Laser-Induced Fluorescence (PLIF1 to PLIF4) units were

147 placed immediately downstream of the fluorimeters to measure the cross-sectional concentration
148 distributions.

149 Fig. 2(c) details the design for the PLIF unit used in this study. The unit consists of a water bath, laser
150 beam, optics and a camera. The pipe passed through the sealed water bath to minimise refraction. A
151 220 mW laser beam, with a wavelength of 532 nm, was used along with a Powell lens and a collimator
152 to generate a vertical laser sheet, illuminating the cross-section of the pipe in the water bath through
153 the glass window at 90° to the direction of flow. A camera (FL3-U3-13Y3M-C, FLIR, USA) was mounted
154 at 45° to the flow direction, capturing the pipe's cross-sectional images through a glass window on the
155 water bath. A long-pass filter (530 nm) was fitted to the camera lens to cut out the laser light. The
156 camera was connected to the computer and controlled through MATLAB (MathWorks Inc., R2022a).
157 The camera parameters were established through initial tests to ensure that, at all locations, the
158 maximum concentration occurring in the pipe was within the image scale. All the components were
159 fixed on a plate, and the entire unit was covered with a black lid to avoid any influence of external
160 light.

161 *Insert Fig. 2.*

162 PLIF and Fluorometer Calibration

163 As the camera in the PLIF unit is 45° to the flow direction, the raw image taken for the circular pipe
164 cross-section appears as an oval shape. Image correction was performed to convert the oval shape to
165 a circle and establish a relationship between image coordinates and real-world coordinates. A 24 mm
166 diameter circle target with a checkerboard pattern of 4 mm squares was inserted into the pipe section
167 for reference images. The images were processed in MATLAB (MathWorks Inc., R2022a) to establish
168 the conversion relationships. Detailed descriptions of the image correction can be found in
169 Supplementary Material A.

170 The direct output from the fluorometers is voltage, and calibrations were performed to determine the
171 relationship between tracer concentration and output voltage. The vertical laser sheet generated by
172 the laser and optics in the PLIF unit is not perfectly uniform, and the calibration with PLIF involves
173 correcting the vertical laser sheet intensity uniformity and converting greyscale image intensity to
174 tracer concentration. Details on the fluorometers and PLIF calibration can be found in Supplementary
175 Material B.

176 Test Programme

177 Headloss measurements were carried out to characterise the pipe hydraulics. Subsequently, temporal
178 concentration profiles and cross-sectional concentration distributions were measured during a series
179 of steady flow conditions and a single accelerating flow condition.

180 Headloss measurements were conducted under 42 steady conditions, covering Reynolds numbers
181 ranging from 700 to 11,000. For each steady flow condition, discharge and headloss were recorded
182 for a duration of 210 s at a frequency of 100 Hz. The mean discharge during this period was then
183 converted to Reynolds number using the viscosity corresponding to the measured water temperature
184 in the pipe, and the friction factor was calculated based on the average head loss using Eq. 1

$$185 \quad f = h_f \left(\frac{d}{L} \right) \left(\frac{2g}{u^2} \right) \quad (1)$$

186 Where f = friction factor; h_f = head loss; L = pipe length; and g = acceleration attributable to gravity.

187 Concentration measurements were performed under 21 steady flow conditions with 5 replicates,
188 covering Reynolds numbers ranging from 700 to 11,000. The valve was opened to the required
189 discharge at the beginning of each test, and to ensure the flow was stable, a 0.5 s duration tracer
190 injection was made 20 s after the test started. The data was recorded for between 60 and 600 s,
191 depending on the design Reynolds number. Data for discharge and fluorometer concentration were

192 collected at 100 Hz. PLIF images were collected at different frequencies, ranging from 10 Hz to 100 Hz,
193 to optimise storage space on the computer.

194 A specific accelerating flow condition was achieved by opening the digital control valve in multiple
195 short steps. Initially, the valve was opened to achieve a design flow of $Re = 1,000$, which was
196 maintained for 20 seconds before the acceleration began. The tracer injection took place for 0.5 s at
197 the start of acceleration. Subsequently, the valve was gradually opened in multiple steps at 0.1s
198 intervals, leading to an effective linear increase in the discharge Reynolds number to 10,500 over 18
199 seconds. Details on the valve operation during the accelerating flow can be found in Supplementary
200 Material C. This acceleration rate was designed to be similar to the lowest acceleration rate (from Re
201 $= 2,700$ to $Re = 47,000$ in 60 seconds) employed by Hart *et al.* (2021), which exhibited disaggregation
202 in temporal concentration profiles. The flow was maintained at $Re = 10,500$ for 30 s until the tracer
203 completely passed all the measurement locations. Ten repeats were conducted with the accelerating
204 flow condition, and all data were logged at a frequency of 100 Hz.

205 As the fluorometers were significantly influenced by the laser in the PLIF units, measurements with
206 fluorometers and PLIF were conducted separately.

207 Uniformity Index

208 PLIF provides the cross-sectional concentration distribution of the tracer. To quantify the degree of
209 cross-sectional mixing within the recorded distribution, a Uniformity Index (UI) for the radial mean
210 concentration distribution was calculated from the corrected and calibrated PLIF images.

211 In this study, the 24 mm diameter pipe area was discretised into 48 circles at 0.25 mm intervals. For
212 each interval, the radial mean concentration, $c_m(r)$, was calculated from all the pixels between
213 adjacent circles, using $c_m(r) = \sum c(r)/N$, where $c(r)$ is the individual pixel concentration and N is
214 the number of pixels within the discretised area. The uniformity of this radial distribution was
215 quantified using a UI , which correlates the radial mean concentration profile, $c_m(r)$, with the area

216 mean concentration, $\overline{c_m(r)}$. This UI (Eq. 2) is insensitive to the absolute value of concentration and
217 the degree of discretisation

$$218 \quad UI = 1 - \frac{\sum (c_m(r) - \overline{c_m(r)})^2}{\sum c_m(r)^2} \quad (2)$$

219 For a perfectly uniform concentration distribution, the UI is 1.0. However, perfect uniformity is not
220 achievable under experimental conditions. To obtain a realistic value of the UI for well-mixed
221 conditions in the experiments, the maximum UI was calculated using the images taken during
222 calibration (where the tracer was believed to be well-mixed) for each PLIF unit. These were found to
223 be > 0.997 for all four units. Any value of the UI less than the well-mixed UI indicates a cross-sectionally
224 non-uniform condition and, the lower the value, the less uniform the distribution. Further details on
225 the UI for ideal synthetic concentration distributions can be found in Supplementary Material D.

226 **RESULTS**

227 **Pipe Hydraulics**

228 Fig. 3(a) presents the relationship between the measured Head Loss and Reynolds number under
229 steady flow conditions. The maximum headloss observed over the 11.8 m pipe is approximately
230 120 mm at $Re = 11,000$, indicating a smooth pipe system. Fig. 3(b) displays the resulting friction factor
231 obtained using Eq.1. The analysis, based on standard laminar/turbulent pipe flow theory, indicates
232 that the flow is laminar for $Re < 2,300$, turbulent for $Re > 3,000$, and transitional flow between.

233 *Insert Fig. 3.*

234 **Steady Flows**

235 *Cross-sectional mean measurement*

236 Fig. 4(a) presents examples of the measurements captured by the fluorometers, and Fig. 4(b) shows
237 the cross-sectional area mean concentration derived from PLIF images under turbulent flow

238 conditions. The shaded red area represents the tracer injection, and the corresponding Reynolds
239 number determined during the test is presented on the secondary y-axis. The measurements from
240 fluorometers and PLIF were independent tests, leading to a minor discrepancy in the mean Reynolds
241 number. However, the Reynolds number was maintained at around 10,400 during both tests. The
242 spike observed in the Reynolds number during the injection phase is attributed to the pressure
243 variation within the pipe.

244 Regarding the concentration profiles, the PLIF profiles are smoother compared to those of the
245 fluorometers. Despite the fluorometer data being collected at a rate of 100 Hz, the physical
246 measurement process within the fluorometers lacks a rapid response (i.e. at 33 HZ). The concentration
247 profiles from both the fluorometers and PLIF share a characteristic slightly skewed Gaussian
248 'distribution', with decreasing peak concentrations and increasing spread with distance along the pipe.

249 Given that the fluorometers are situated upstream of the PLIF units, it was expected that the
250 fluorometers would yield higher peak concentrations compared to PLIF. This trend is evident for the
251 first three measurement locations. For the fourth fluorometer (F4), the fluorometer measurement
252 reads 4 ppb while the area mean concentration from PLIF registers at 7 ppb. Despite the fluorometer
253 measurements not confirming mass balance, the shape of the temporal profiles was captured by both
254 instruments and the estimated longitudinal dispersion coefficient is consistent.

255 Similar results were obtained across the range of tests conducted under turbulent flow conditions. In
256 light of this consistency, it is inferred that the fluorometers deliver a reliable measurement of the area
257 mean concentration in turbulent flow conditions from which the longitudinal dispersion can be
258 quantified from the method of moment.

259 Fig. 4(c) and (d) present the results from fluorometers and PLIF under a condition close to transitional
260 flow (i.e. $Re \approx 3500$). It should be noted that for better a representation of the concentration profiles,
261 the ranges of the y-axis for the two subplots are different. Despite the fluorometers registering a

262 higher area mean concentration than PLIF, the shape of the concentration profiles measured by both
263 instruments is quite consistent.

264 Fig. 4(e) and (f) present the results from fluorometers and PLIF under laminar flow conditions. It should
265 be noted that for better a representation of the concentration profiles, the ranges of the y-axis for the
266 two subplots are different. The Reynolds number was maintained steady during both tests and, as the
267 pressure in the pipe was close to the injection pressure, the sudden increase in Reynolds number due
268 to injection was not visible. It is notable that under this laminar flow condition, there is a substantial
269 disagreement in the area mean concentration measurements between the fluorometers and PLIF. The
270 fluorometers consistently reported much higher concentrations. For instance, F2 recorded a peak
271 concentration of 23 ppb, while the area mean concentration derived from PLIF1 yielded a peak
272 concentration of only 8 ppb.

273 This pattern of fluorometers reporting higher concentrations was found consistently across all the
274 laminar flow conditions. This discrepancy might be attributed to the fact that when the tracer is not
275 cross-sectionally well-mixed, the fluorometers do not account for the optical bias. The shape of the
276 temporal concentration profiles measured by the PLIF was, as expected, non-Gaussian and unlike the
277 fluorometers, the PLIF technique was able to capture the elongated tails. Overall, the comparison with
278 the area mean concentration derived from PLIF images suggests that fluorometers do not provide a
279 representative measurement of the cross-sectional area mean concentration under laminar flow
280 conditions.

281 The shape of the temporal concentration profiles is more skewed and spread at low Reynolds numbers
282 and it becomes less spread and close to a Gaussian form with the increase of Reynolds number.

283 *Insert Fig. 4.*

284 *Cross-sectional concentration distribution*

285 Fig. 5(a) shows the cross-sectional concentration distribution at selected times measured at the four
286 PLIF locations in turbulent flow ($Re = 10,408$). The shade of red reflects the tracer concentration, but
287 it should be noted that the range decreases from upstream locations to downstream locations due to
288 the effects of longitudinal dispersion. The black circle indicates the 24 mm diameter pipe boundary.
289 The three selected times in Fig. 5(a) correspond to the time when the tracer arrived at the
290 measurement locations; the peak area mean concentration; and after the majority of the tracer had
291 passed the measurement locations. The plots in the same row are from the same measurement
292 location.

293 The effect of shear stress at the pipe boundary was evident at all the locations for this flow condition.
294 As the tracer arrives, the concentration is primarily at the centre of the pipe, but as the tracer passes
295 through, higher tracer concentration becomes prominent at the pipe boundary. The tracer is cross-
296 sectionally well-mixed at all the measurement locations and it is almost uniformly distributed at the
297 area mean concentration peaks, which indicates a high level of radial mixing.

298 Fig. 5(b) presents the corresponding temporal profiles for the uniformity index of the same test. The
299 horizontal line on the y-axis is the lowest uniformity index calculated from the calibration images and
300 is considered the uniformity index corresponding to well-mixed conditions. The shaded area is the
301 area mean concentration (secondary y-axis), and the three vertical lines correspond to the three
302 selected times shown in Fig. 5(a).

303 The uniformity index for the three selected times is consistent with the distributions shown in Fig.
304 5(a), demonstrating a more uniform distribution at the area mean concentration peaks (i.e. achieving
305 a well-mixed condition at all the locations at peaks). The temporal uniformity index profiles at the four
306 locations exhibit a trend of increasing with area mean concentration and maintaining a high value
307 during the majority of the time of tracer passing, before decreasing towards the tail of the profile. The

308 tracer reached a condition, being cross-sectionally well-mixed (e.g. $UI > 0.95$), at all the measurement
309 locations during the test and was better mixed at the downstream locations. PLIF1 and PLIF2 recorded
310 26.15% and 40.18 % of the test duration at the well-mixed condition, and PLIF3 and PLIF4 recorded
311 55.46% and 72.51%. These results confirm that it is not possible to have complete cross-sectional
312 mixing throughout the complete duration of a tracer cloud, as the leading and trailing edges will
313 always exhibit aspects of the longitudinal velocity profile, even under turbulent flow conditions.

314 *Insert Fig. 5.*

315 Fig. 6(a) presents the cross-sectional concentration distribution for the laminar flow condition ($Re =$
316 822). At the first measurement location (PLIF1), a clear progression of the tracer distribution is
317 presented from a concentrated patch in the pipe centre gradually spreading out to form an annular
318 shape extending towards the pipe edges. This trend is also evident at all downstream locations, but
319 as the tracer is slightly more dense than the water, the cloud moves vertically downwards with
320 distance along the pipe. The tracer distribution at laminar flow conditions presented in Fig. 6(a) is
321 caused by the velocity distribution in the pipe, in which the tracer in the pipe centre travelled faster
322 than the tracer near the pipe boundary, combined with very little radial mixing. Over this short
323 distance (e.g. 5.5 m), the tracer is not cross-sectionally well-mixed (e.g. $UI < 0.6$), as shown by the
324 corresponding uniformity index profiles, Fig. 6(b).

325 Across all four measurement locations, there was a consistent trend in the uniformity index. In the
326 case of PLIF1, the uniformity index exhibited an increase towards the tail end of the concentration
327 profiles, primarily influenced by background noise levels at low concentrations. At PLIF3 and PLIF4, a
328 minor secondary peak in the uniformity index was evident. This observation may be attributed to the
329 asymmetrical shape of the tracer concentration and the fact that the centre of the tracer patch is not
330 aligned with the pipe's centre. It is important to note that the uniformity index does not define the
331 shape of the concentration distribution: there are instances where uniformity index values are

332 identical, but the shape of the distribution is different. However, the uniformity index does serve as
333 an indicator of how well the tracer is cross-sectionally mixed.

334 In laminar flow, the radial mixing is dominated by molecular diffusion, around 10^{-10} m²/s, which
335 requires long travel times to achieve fully mixed conditions. The non-uniform distributions also caused
336 inaccurate measurement of area mean concentrations from the Fluorometers. Fluorometers are
337 designed to measure only the areas containing tracer; at this condition, due to a large proportion of
338 the pipe cross-section not containing tracer, the fluorometers do not accurately measure area mean
339 concentration, and this led to the significantly elevated area mean concentrations in the fluorometers
340 as shown in Fig. 4(c).

341 *Insert Fig. 6.*

342 Fig. 7 shows the uniformity index at the peak area mean concentration for all the steady flow
343 conditions. It is evident that at laminar flow conditions (e.g. $Re < 2,300$), UI at the peak concentration
344 is notably low (i.e. $UI_{peak} < 0.8$), which indicates poor radial mixing. However, as the Reynolds number
345 increases, UI_{peak} increases, approaching well-mixed conditions and suggesting greater radial mixing. At
346 transitional and turbulent flow conditions ($Re > 2,300$), the uniformity index for PLIF4 is closer to the
347 well-mixed uniformity index than the upstream locations. This indicates that well-mixed conditions
348 did not occur instantaneously, but the tracer became more uniformly distributed as it travelled
349 downstream.

350 *Insert Fig. 7.*

351 Accelerating Flow

352 *Cross-sectional mean measurement*

353 Fig. 8(a) shows the measurements from the fluorometers during the accelerating flow, with the
354 secondary y-axis showing the measured Reynolds number during the test. In this test, the flow was
355 accelerated linearly from $Re = 1,200$ to $Re = 10,000$ between 20 s and 38 s, with the tracer injection at
356 the start of the acceleration. The measured temporal concentration profiles at all four locations
357 showed two peaks, with the concentration at the first peak being higher than the second. Due to
358 dispersion effects, the downstream peaks are lower and the distribution exhibits a greater spread.

359 Fig. 8(b) shows the derived cross-sectional area mean concentration profiles from the PLIF images for
360 an identical accelerating flow test. Area mean PLIF distributions also exhibited two peaks at all the
361 locations, but the area mean concentration was less than half the values given by the fluorometers
362 (e.g. 15 ppb versus 42 ppb at the first measurement location). This indicates that the non-uniform
363 concentration distribution experienced in the laminar flow conditions also influenced the accuracy of
364 the fluorometer measurements during accelerating flow. At downstream locations, the temporal
365 separation between the two peaks is more distinct, suggesting that the tracer contributing to the first
366 peak was travelling faster than the second and the differential velocity between the peaks increased.

367 The temporal concentration profiles exhibited two peaks in all 10 repeat tests under the accelerating
368 flow conditions, which is consistent with the findings of Hart *et al.* (2021). It should be noted that in
369 this study two peaks were consistently observed from all the PLIF measurements, even at the first
370 measurement location, and the disaggregation from a single upstream peak to downstream multiple
371 peaks was not evident in the PLIF data. This can be attributed to the differences from Hart *et al.* (2021)
372 in both the initial Reynolds number and the distance from the injection point to the first measurement
373 location. The initial Reynolds number in this study was around 1,200, lower than the 2,700 used by
374 Hart *et al.* (2021). A lower initial Reynolds number implies that the distance to detect the effects of

375 differential longitudinal advection is shorter and in the current work the closest PLIF was 0.834 m from
376 the injection point in comparison to the 0.5 m from the injection point in Hart *et al.* (2021).

377 The shaded blue area in Fig. 8(a) and (b) is the region where the mean flow measured for steady flow
378 conditions was within the transitional flow regime. By the time the tracer reached the first PLIF
379 measurement location (PLIF1, around 25 s), the flow within the pipe was turbulent.

380 *Insert Fig. 8.*

381 *Cross-sectional concentration distribution*

382 Fig. 9(a) illustrates the cross-sectional concentration distribution at four PLIF measurement locations
383 during the accelerating flow. The selected times correspond to when the area mean concentration
384 reached its first peak, its second peak, and one instance between the two peaks.

385 At PLIF1, the first peak showed a cross-sectional distribution that was not well-mixed with the tracer
386 concentrated primarily in the central region of the pipe. At the second peak, the tracer reached the
387 pipe boundary accompanied by eddies in the central area. Between the two peaks at $t = 28.01$ s, the
388 concentration distribution took on an annular shape near the pipe boundary, similar to the
389 distribution seen in the late-stage of laminar flows. At PLIF2 and PLIF3, similar concentration
390 distributions were recorded. However, at PLIF4, the tracer exhibited a uniform, well-mixed cross-
391 sectional distribution throughout the duration of the tracer.

392 The concentration distribution provides insights into the behaviour of the tracer during the
393 accelerating flow. The tracer located in the pipe centre contributes to the first peak of the temporal
394 profile; the tracer located at pipe boundary contributes to the second peak. The tracer becomes cross-
395 sectionally well-mixed due to rapid radial mixing during turbulent flow conditions. Due to the velocity
396 distribution within the pipe and the acceleration of the flow, the tracer in the pipe's central region
397 accelerates more rapidly than the tracer at the pipe's boundary, leading to a greater separation

398 between the two peaks at downstream locations, as shown in the area mean temporal concentration
399 profiles in Fig. 8(b).

400 Fig. 9(b) is the temporal profile of the *UI* with vertical lines indicating the selected times in Fig. 9(a);
401 Table 1 summarises the conditions of the two peaks presented in Fig. 8(b).

402 *Insert Table 1.*

403 An interesting observation is that, despite the mean flow in the pipe being turbulent ($Re = 4,626$) when
404 the tracer arrived at the first measurement location at 26.12 s, the tracer was not cross-sectionally
405 well-mixed. It wasn't until around 37.31 s ($Re = 10,147$) at PLIF4, that the first patch of tracer became
406 cross-sectionally well-mixed, whilst the second patch of tracer was cross-sectionally well-mixed at
407 PLIF2 at 31.34 s ($Re = 7,404$). This phenomenon may be attributed to spatial velocity development and
408 cross-sectional velocity distributions. Whilst the mean flow exhibited rapid acceleration due to the
409 valve opening, it remains uncertain whether this acceleration happened simultaneously at all locations
410 within the pipe. A delayed change to turbulent flow conditions at downstream locations could result
411 in non-uniform cross-sectional tracer distributions, despite the mean discharge from the pipe
412 suggesting fully turbulent flow conditions. The first cloud of tracer is located at the pipe centre and to
413 achieve cross-sectional well-mixed conditions requires sufficient radial mixing. Under accelerating
414 flows, the radial velocity gradient towards the centre of the pipe may not increase sufficiently for this
415 to occur. However, the second cloud of tracer is located close to the pipe boundary, and this tracer
416 attains cross-sectionally well-mixed conditions at an earlier stage of acceleration from higher radial
417 mixing caused by greater velocity gradients at the boundary. Clearly, detailed spatial and temporal
418 velocity measurements are needed to confirm this hypothesis.

419 *Insert Fig. 9.*

420 **DISCUSSION**

421 The comparison between fluorometer and PLIF measurements highlighted a significant limitation,
422 specifically during laminar flow conditions, when the tracer in the pipe was not uniformly mixed across
423 the pipe cross-section. Under such flows, the fluorometers did not yield reliable measurements of the
424 cross-sectional area mean concentration. This suggests that the method of sampling tracer during
425 laminar flow can significantly impact the accuracy of experimental data and subsequent determination
426 of longitudinal dispersion coefficients. The measured concentration from fluorometers at laminar
427 flows, e.g. in Hart *et al.* (2016), may not be representative of pipe cross-sectional mean concentration.
428 In some studies (Piazza *et al.*, 2020, & 2022; Romero-Gomez and Choi, 2011) where the tracer was
429 sampled at the pipe wall, it may lead to an inaccurate representation of tracer concentration during
430 laminar flow.

431 The influence of the sampling method extends to applications involving water quality analysis (e.g.
432 inorganics, disinfectant and biofilm) in the main water distribution network (e.g. Abokifa *et al.* 2016;
433 Prévost *et al.* 1997). Evaluating the representativeness of collected data, particularly during low flows,
434 requires careful consideration of the degree of cross-sectional mixing. This factor becomes critical in
435 determining the accuracy and reliability of water quality assessments derived from sampled data
436 within the distribution network.

437 PLIF measurements offer a more accurate representation of the pipe's cross-sectional mean
438 concentration than single-point sampling. However, implementing this technique in live water
439 distribution networks may be unfeasible. Nonetheless, the PLIF data collected in this study holds
440 substantial value for the broader community within the field, providing valuable insights into pipe
441 cross-sectional concentration distributions and area mean concentration that can guide future
442 research and development in this area.

443 EPANET has long been used to study hydraulics and water quality in water distribution systems. The
444 inclusion of dispersion effects in the conventional advection-based EPANET model has proven to

445 improve its predictions, as evidenced by comparisons between modelled and experimentally
446 measured data (Burkhardt *et al.* 2020; Piazza *et al.* 2020, 2022; Shang *et al.* 2023). The refinement of
447 numerical models often relies on experimental data to verify model accuracy. In this context, the PLIF
448 dataset gathered in this study serves as a source of pipe cross-sectional mean concentration data,
449 facilitating further validation of the 1D model. Additionally, the cross-sectional concentration
450 distribution offers an opportunity for extended validation of 2D models which are essential to describe
451 contaminant interactions with boundary biofilms and pipe material.

452 **CONCLUSIONS**

453 Four fluorometers and PLIF units were used to measure the cross-sectional area mean temporal
454 concentration profiles resulting from a single pulse of tracer injected at an upstream location under
455 steady and accelerating flows. Observations in steady turbulent flows showed that the fluorometers
456 deliver a reliable measurement of the area mean concentration. However, due to low radial mixing,
457 the fluorometers do not offer an accurate measurement of the cross-sectional area mean
458 concentration under laminar flow conditions.

459 PLIF provides, for the first time, the opportunity for visualisation of pipe cross-sectional tracer
460 concentration distribution development and evolution due to radial mixing at different steady flow
461 conditions. It showed that the tracer is cross-sectionally well-mixed at all the measurement locations
462 in turbulent flows. In laminar flows, a clear progression was observed with an initial distribution at the
463 pipe centre, gradually spreading to form an annular shape extending towards the pipe wall. This is a
464 result of the velocity distribution and the low radial mixing.

465 In the accelerating flow condition, the temporal concentration profiles measured at all the
466 downstream locations showed two peaks with the first peak being higher than the second. The cross-
467 sectional PLIF concentration distributions revealed that at the first measurement location, the two
468 peaks were not cross-sectionally well-mixed, but at a downstream location, the two peaks became

469 cross-sectionally well-mixed. This provides a significant improvement in understanding the temporal
470 and spatial variations in radial mixing during accelerating pipe flows.

471 The disaggregation from a single upstream peak to downstream multiple peaks was observed in this
472 study and is consistent with the observations of Hart et al. (2021). The new cross-sectional PLIF data
473 provided the opportunity to quantify the difference in the spatial distribution of the tracer at the peaks
474 for the first time. The cause of the disaggregation requires detailed velocity measurements to identify
475 the underlying mechanisms.

476 Evaluating the representativeness of collected data, particularly during low flows and where the water
477 sample is taken from a single point at the pipe wall, requires careful consideration of the degree of
478 cross-sectional uniformity. The PLIF data collected in this study provides an accurate representative
479 measurement of pipe cross-sectional mean concentration and holds substantial value for model
480 validations.

481 **DATA AVAILABILITY STATEMENT**

482 The data, models, and code generated or used during the study are available in a repository or
483 online in accordance with funder data retention policies from Peng *et al.* (2024)
484 (<https://doi.org/10.15131/shef.data.23735919>).

485 **ACKNOWLEDGEMENTS**

486 The authors would like to thank Joseph Milner, who provided technical support for all the laboratory
487 studies conducted at the University of Sheffield. Additional appreciation was also given to Professor
488 Shuisheng He and Oliver Cooper for their generous provision and assistance in using their lab space.
489 This work was supported by the EPSRC Grant No. EP/P012027/1.

490 For the purpose of open access, the author has applied a Creative Commons Attribution (CC BY) licence
491 to any Author Accepted Manuscript version arising.

492 **SUPPLEMENTARY MATERIALS**

493 Supplementary Materials A, B and C are available online in the ASCE Library (ascelibrary.org).

494 **REFERENCE**

495 Abokifa, A. A., Yang, Y. J., Lo, C. S., and Biswas, P. (2016). "Water quality modeling in the dead end
496 sections of drinking water distribution networks." *Water Research*, Pergamon, 89, 107–117.

497 Buchberger, S. G., Carter, J. T., Lee, Y., and Schade, T. G. (2003). "Random demands, travel times and
498 water quality in deadends." *Rep. No. 90963F:470*, Denver: American Water Works Association
499 Foundation.

500 Burkhardt, J. B., Woo, H., Mason, J., Shang, F., Triantafyllidou, S., Schock, M. R., Lytle, D., and
501 Murray, R. (2020). "Framework for Modeling Lead in Premise Plumbing Systems Using
502 EPANET." *Journal of Water Resources Planning and Management*, American Society of Civil
503 Engineers (ASCE), 146(12), 04020094.

504 Crimaldi, J. P. (2008). "Planar laser induced fluorescence in aqueous flows." *Experiments in Fluids*,
505 Springer, 44(6), 851–863.

506 Fischer, H. B., List, J. E., Koh, C. R., Imberger, J., and Brooks, N. H. (1979). *Mixing in Inland and*
507 *Coastal Waters*. Elsevier.

508 Flint, L. F., and Eisenklam, P. (1969). "Longitudinal gas dispersion in transitional and turbulent flow
509 through a straight tube." *The Canadian Journal of Chemical Engineering*, John Wiley & Sons,
510 Ltd, 47(2), 101–106.

511 Fowler, F. C., and Brown, G. G. (1943). *Contamination by Successive Flow in Pipe Lines*. American
512 institute of chemical engineers.

513 Greenblatt, D., and Moss, E. A. (2004). "Rapid temporal acceleration of a turbulent pipe flow."
514 *Journal of Fluid Mechanics*, Cambridge University Press, 514, 65–75.

515 Harry, A.J., Pearson, J.M., Guymer, I. and Potter, R., (1996). "Development of an In-situ

516 Concentration Measurement Technique to Investigate Vertical Mixing Processes in the Coastal
517 Zone." *Proceedings of Second International Conference on Hydrodynamics*, Hong Kong, 16-19
518 December, 1007–1012.

519 Hart, J. R., Guymer, I., Sonnenwald, F., and Stovin, V. R. (2016). "Residence Time Distributions for
520 Turbulent, Critical, and Laminar Pipe Flow." *Journal of Hydraulic Engineering*, 142(9), 1–10.

521 Hart, J., Sonnenwald, F., Stovin, V., and Guymer, I. (2021). "Longitudinal Dispersion in Unsteady Pipe
522 Flows." *Journal of Hydraulic Engineering*, 147(9), 1–12.

523 He, S., and Jackson, J. D. (2000). "A study of turbulence under conditions of transient flow in a pipe."
524 *Journal of Fluid Mechanics*, Cambridge University Press, 408, 1–38.

525 Keyes, J. J. (1955). "Diffusional film characteristics in turbulent flow: Dynamic response method."
526 *AIChE Journal*, John Wiley & Sons, Ltd, 1(3), 305–311.

527 Kurokawa, J., and Morikawa, M. (1986). "Accelerated and Decelerated Flows in a Circular Pipe : 1st
528 Report, Velocity Profile and Friction Coefficient." *Bulletin of JSME*, The Japan Society of
529 Mechanical Engineers, 29(249), 758–765.

530 Lee, J., Burkhart, J.B., Buchberger, S., Grayman, W., Haxton, T, Janke, R., Murray, R. and Platten, W.E.
531 (2023). "*Premise Plumbing Modeling*." ASCE, Env. & Water Resources Institute.

532 LeChevallier, M. W., Gullick, R. W., Karim, M. R., Friedman, M., and Funk, J. E. (2003). "The potential
533 for health risks from intrusion of contaminants into the distribution system from pressure
534 transients." *Journal of Water and Health*, IWA Publishing, 1(1), 3–14.

535 Mathieu, J., and Scott, J. (2000). *An introduction to turbulent flow*. Cambridge University Press.

536 Peng, Z., Stovin, V., and Guymer, I. (2024). "Cross-sectional solute concentration distribution in
537 steady and accelerating pipe flows". The University of Sheffield, 10.15131/shef.data.23735919.

538 Piazza, S., Mirjam Blokker, E. J., Freni, G., Puleo, V., and Sambito, M. (2020). "Impact of diffusion and
539 dispersion of contaminants in water distribution networks modelling and monitoring." *Water*

540 *Supply*, IWA Publishing, 20(1), 46–58.

541 Piazza, S., Sambito, M., and Freni, G. (2022). “A Novel EPANET Integration for the Diffusive–
542 Dispersive Transport of Contaminants.” *Water 2022, Vol. 14, Page 2707*, Multidisciplinary
543 Digital Publishing Institute, 14(17), 2707.

544 Prévost, M., Rompré, A., Baribeau, H., Coallier, J., and Lafrance, P. (1997). “Service lines: Their effect
545 on microbiological quality.” *Journal - American Water Works Association*, American Water
546 Works Association, 89(7), 78–91.

547 Romero-Gomez, P., and Choi, C. Y. (2011). “Axial Dispersion Coefficients in Laminar Flows of Water-
548 Distribution Systems.” *Journal of Hydraulic Engineering*, American Society of Civil Engineers,
549 137(11), 1500–1508.

550 Rossman, L. A. 2000. EPANET 2: Users manual. Washington, DC: USEPA

551 Shang, F., Burkhardt, J. B., and Murray, R. (2023). “Random Walk Particle Tracking to Model
552 Dispersion in Steady Laminar and Turbulent Pipe Flow.” *Journal of Hydraulic Engineering*,
553 149(7), 1–9.

554 Swarnkar, K., Nikam, V., Gupta, K., and Pearson, J. M. (2022). “Review of the state-of-the-art for
555 monitoring urban drainage water quality using rhodamine WT dye as a tracer.”
556 <https://doi.org/10.1080/09715010.2022.2098682>, Taylor & Francis.

557 Taylor, G. I. (1954). “The dispersion of matter in turbulent flow through a pipe.” *Proceedings of the*
558 *Royal Society of London. Series A. Mathematical and Physical Sciences*, The Royal Society
559 London, 223(1155), 446–468.

560 van Cruyningen, I., Lozano, A. and Hanson, R.K., (1990). “Quantitative Imaging of Concentration by
561 Planar Laser Induced Fluorescence. ” *Experiments in Fluids*, Vol. 10, pp 41-49.

562 Wilson, J. F., Cobb, E. D., and Kilpatrick, F. A. (1986). *Fluorometric procedures for dye tracing*.
563 Department of the Interior, US Geological Survey.

Fig. 1. Disaggregation in accelerating flow (from Hart *et al.*, 2021).

Fig. 2. Experimental set-up and instrumentation; (a) pipe test section (not to scale); (b) 2D PLIF unit (plan view); (c) Snapshot of food dye injection.

Fig. 3. Variation of (a) head loss and (b) friction factor with Reynolds number.

Fig. 4. Temporal concentration profiles at steady flow conditions; (a) measured by fluorometers at $Re = 10,452$; (b) area mean concentration profiles derived from 2D PLIF images at $Re = 10,408$; (c) measured by fluorometers at $Re = 861$; (d) area mean concentration profiles derived from 2D PLIF images at $Re = 822$.

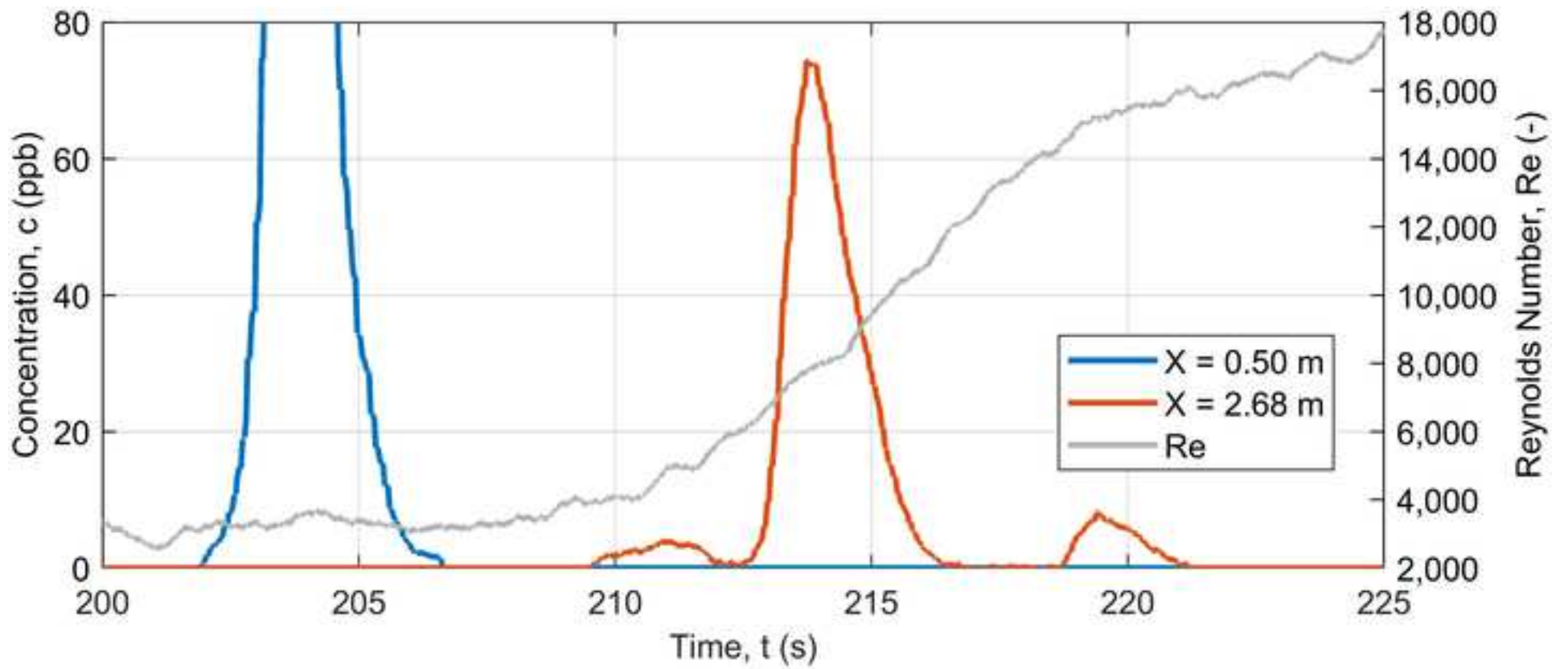
Fig. 5. Steady flow condition at $Re = 10,408$; (a) cross-sectional concentration distribution for selected times; (b) temporal uniformity index profiles derived from PLIF images, the vertical lines correspond to the selected times in Fig. 4(a).

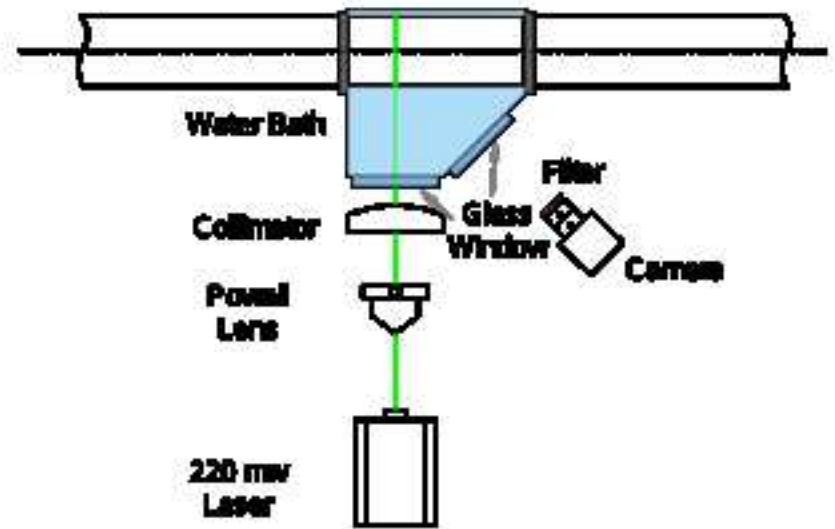
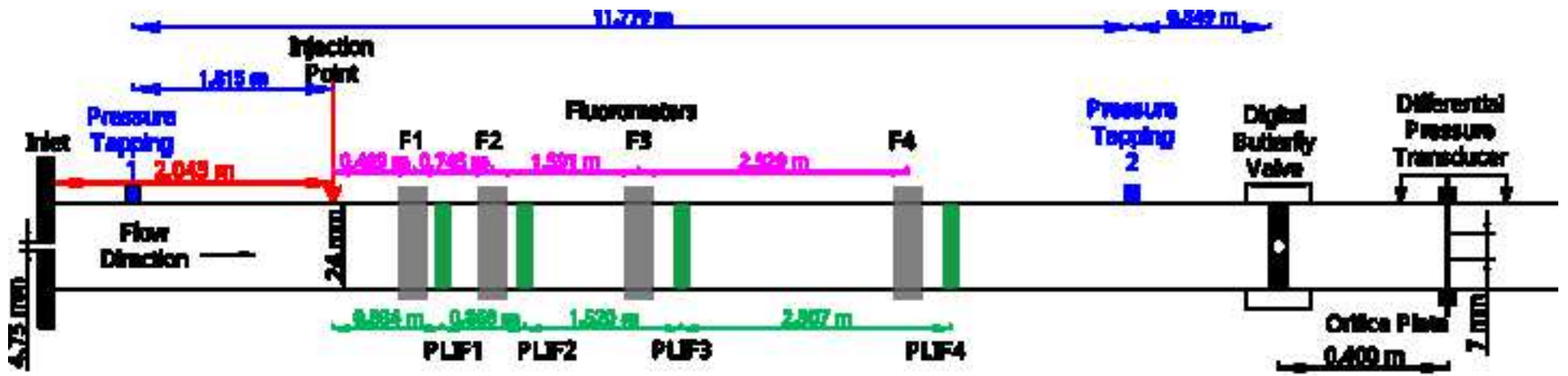
Fig. 6. Steady flow condition at $Re = 822$; (a) cross-sectional concentration distribution for selected times; (b) temporal uniformity index profiles derived from PLIF images (the vertical lines correspond to the selected times in Fig. 5(a)).

Fig. 7. Variation of uniformity index at peak area mean concentrations with Reynolds number.

Fig. 8. Temporal concentration profiles at the accelerating flow; (a) measured by fluorometers; (b) area mean concentration derived from 2D PLIF images.

Fig. 9. Accelerating flow condition; (a) cross-sectional concentration distribution for selected times; (b) temporal uniformity index profiles derived from PLIF images at the accelerating flow, the vertical lines correspond to the selected times in Fig. 8(a).

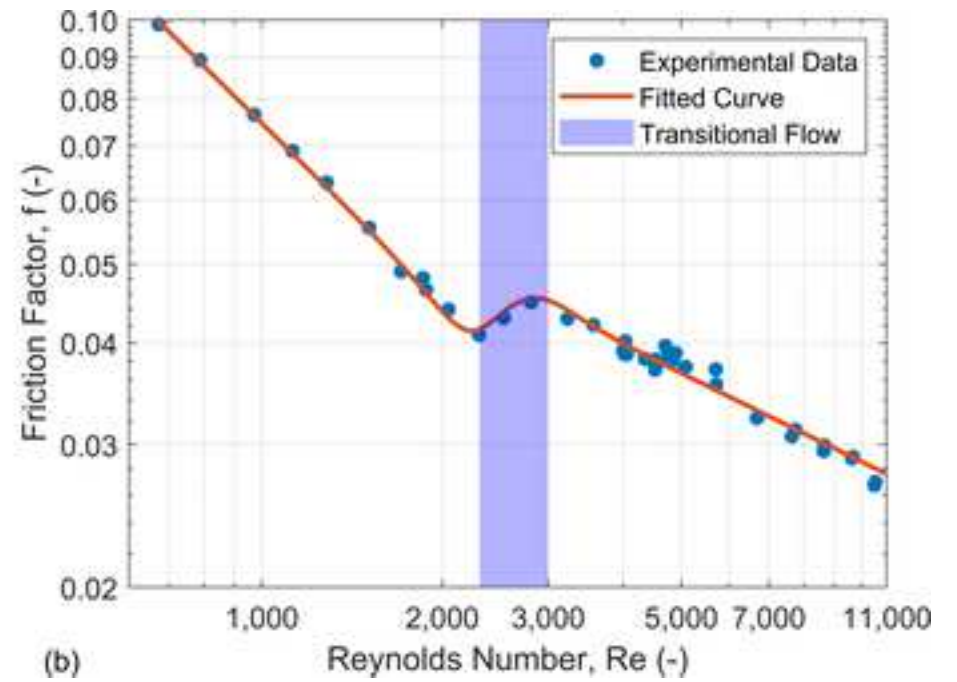
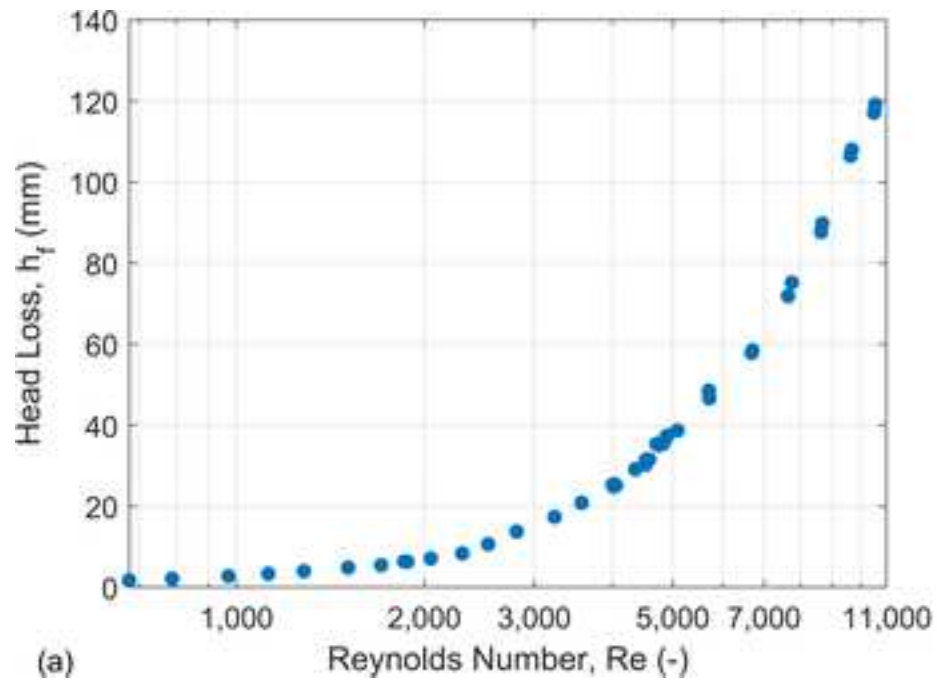


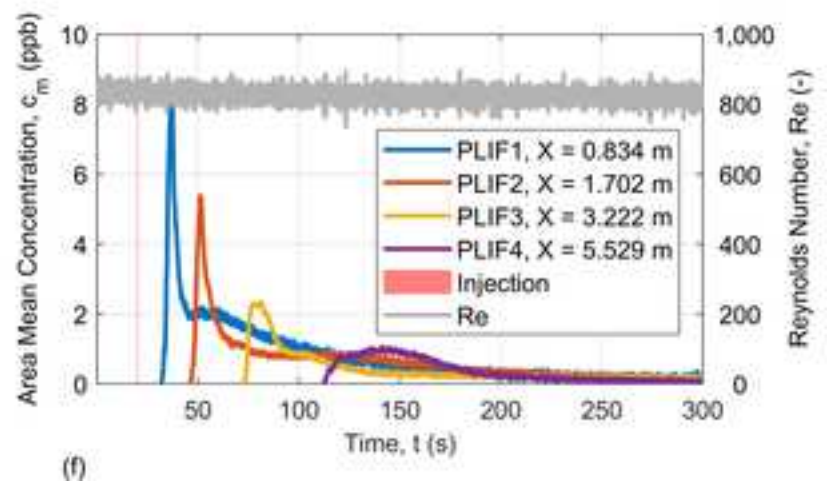
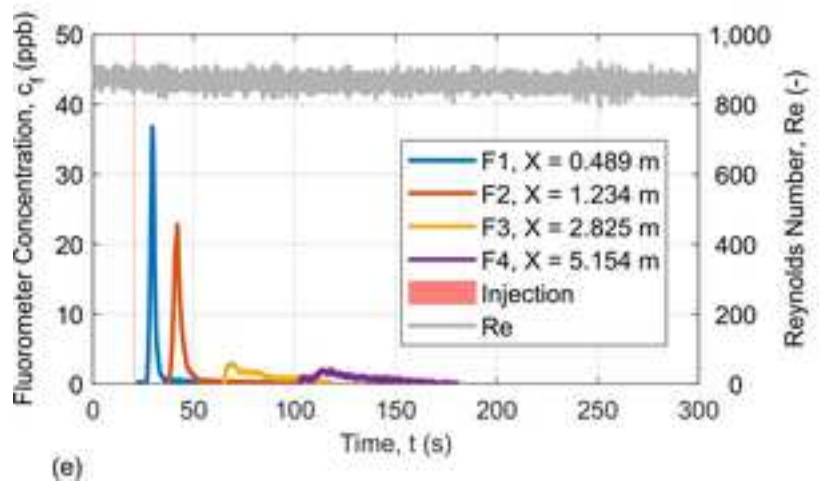
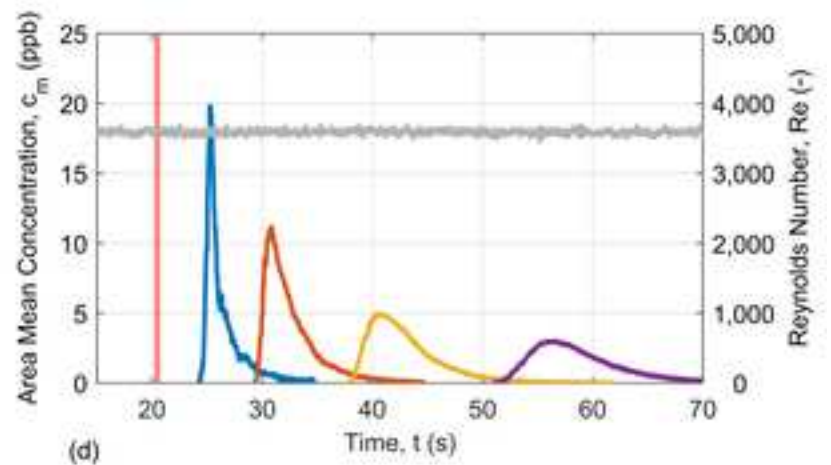
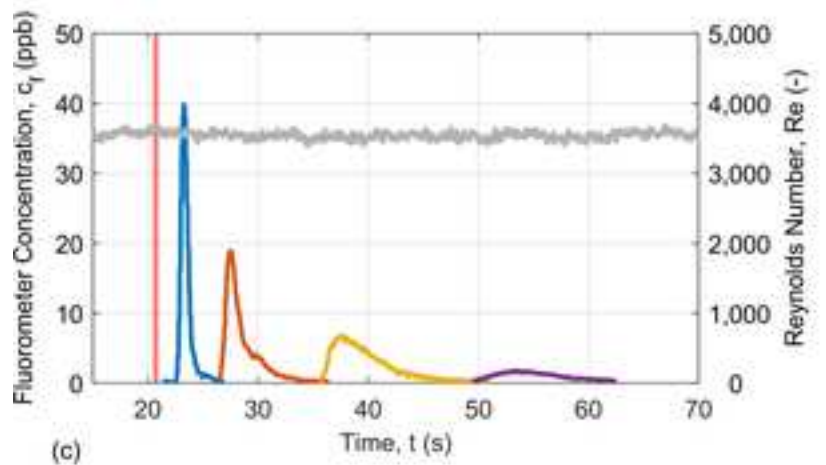
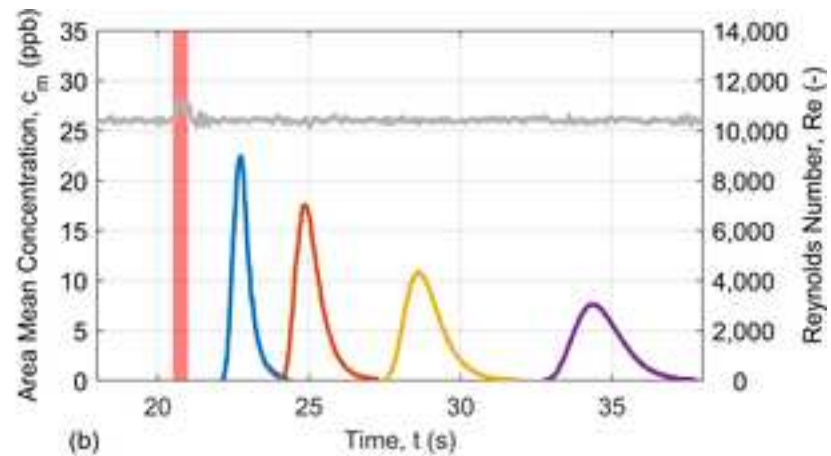
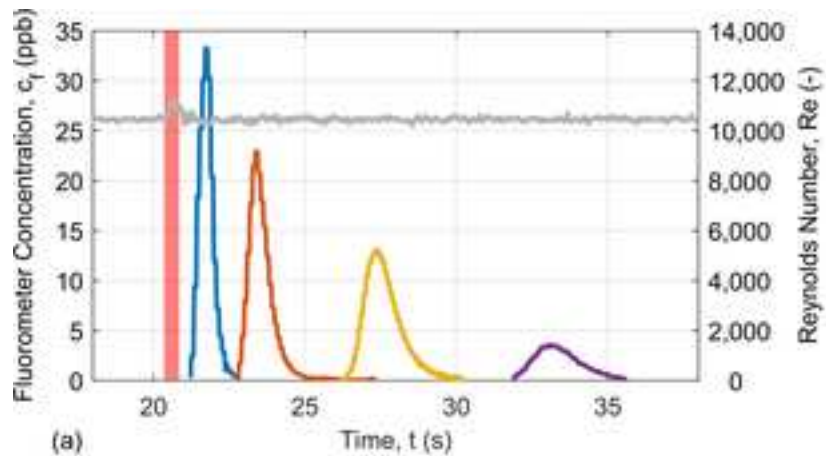


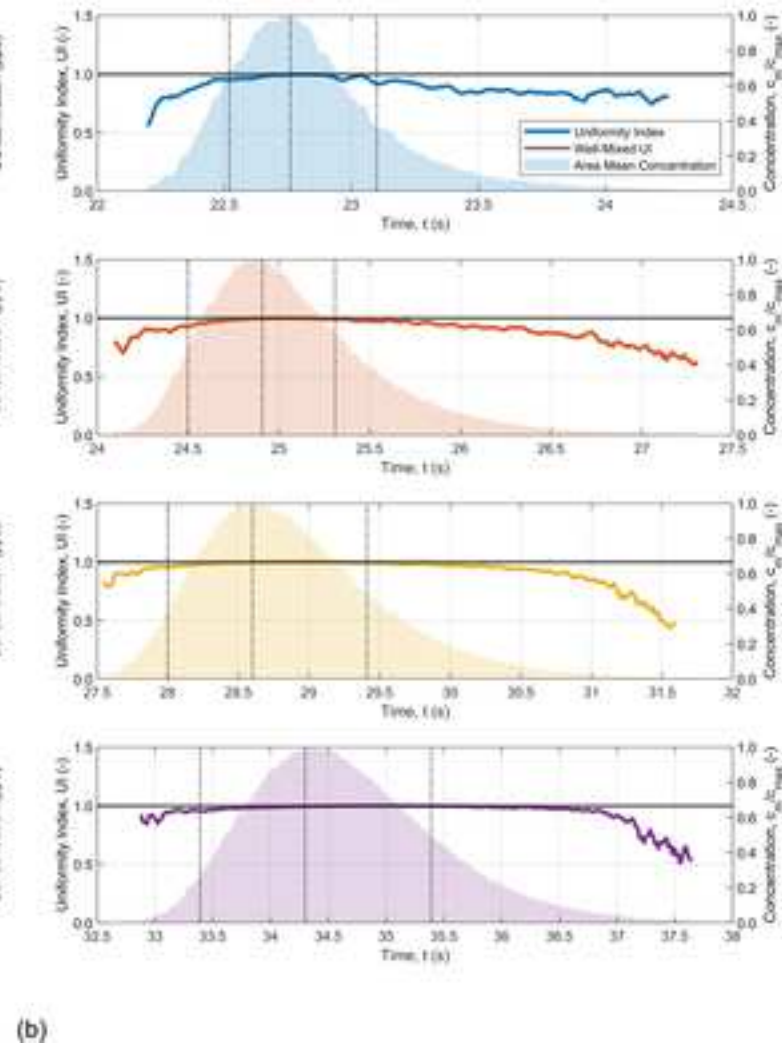
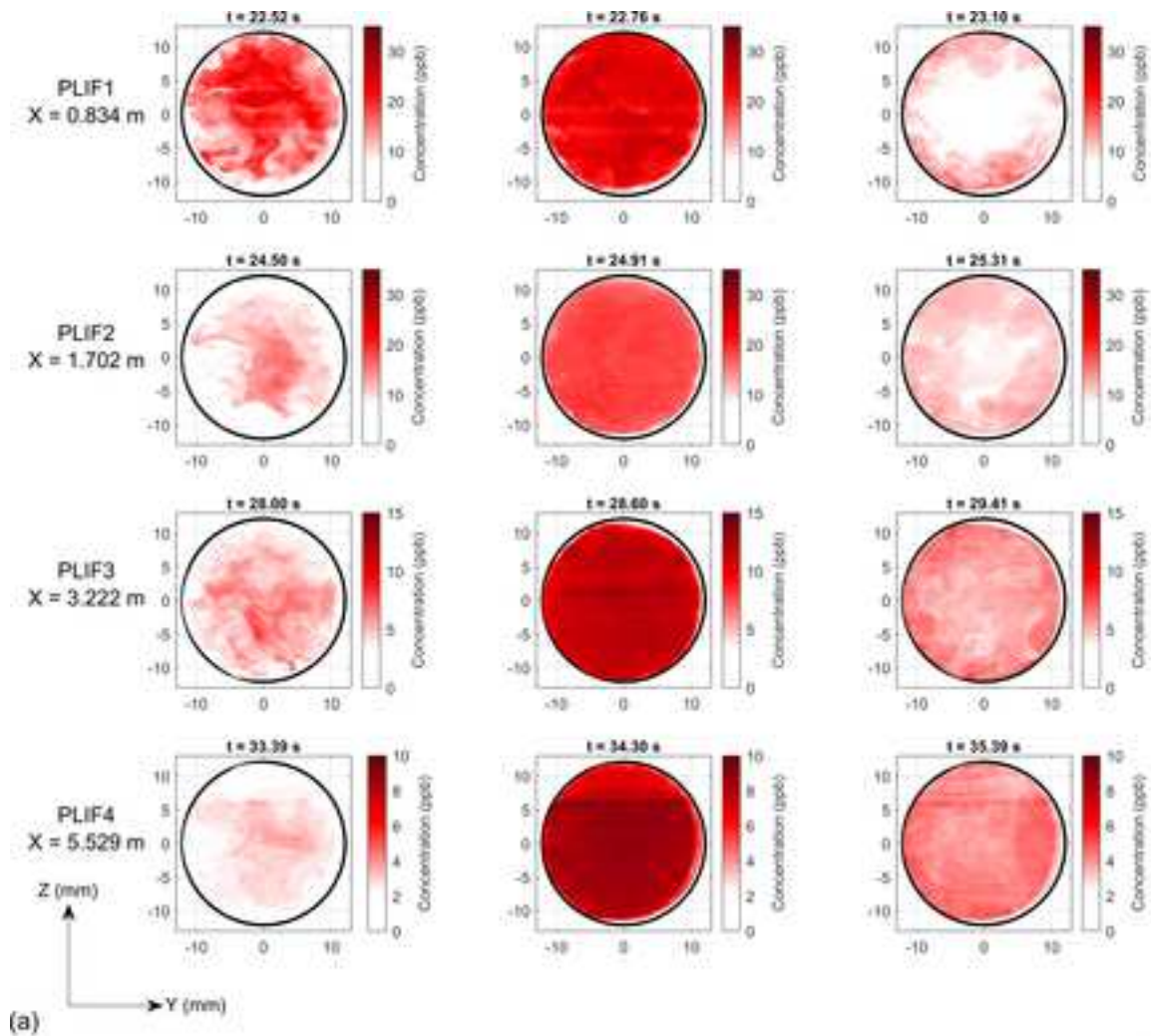
6

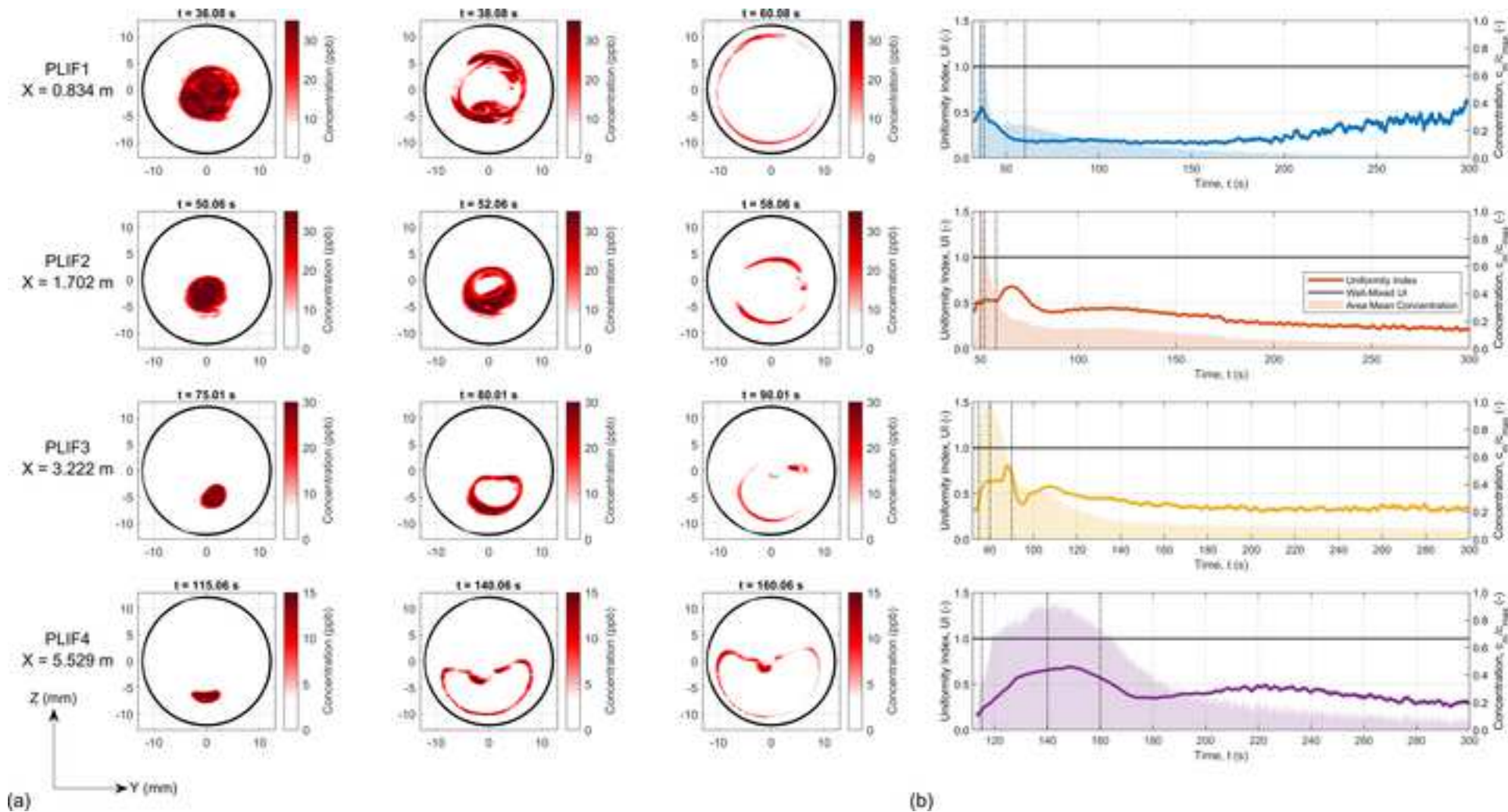
6

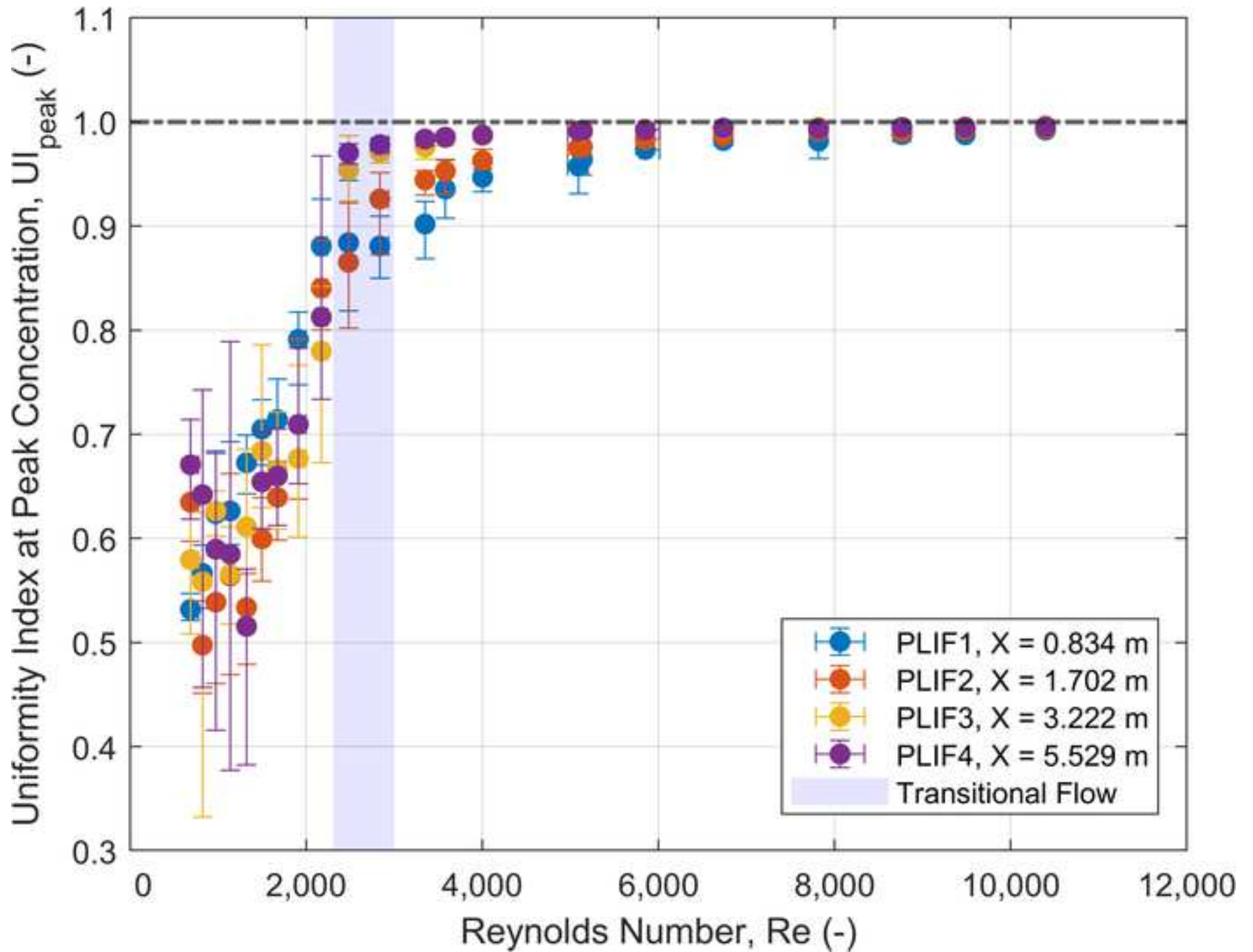
6

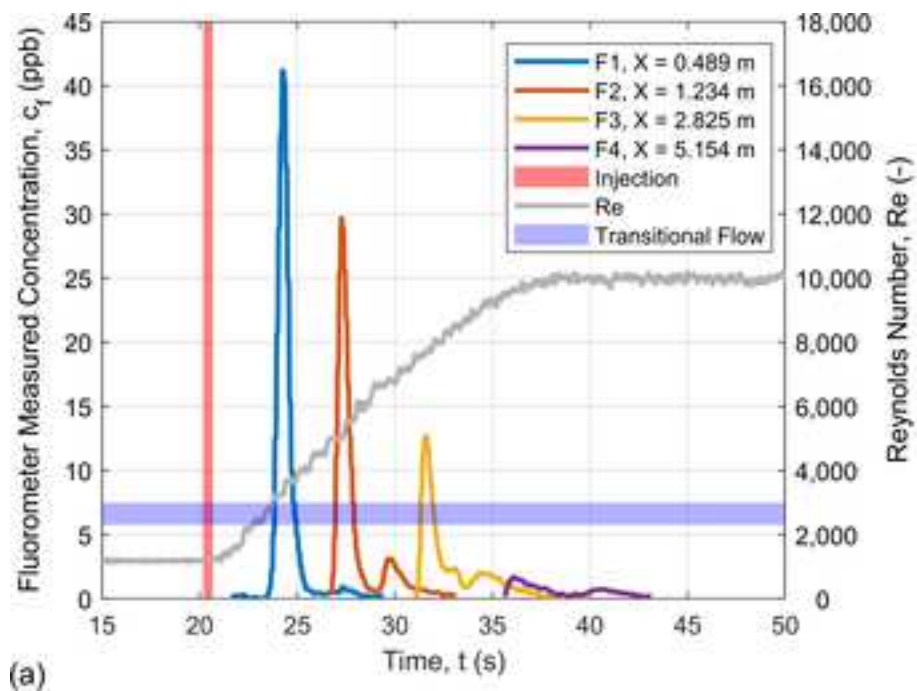




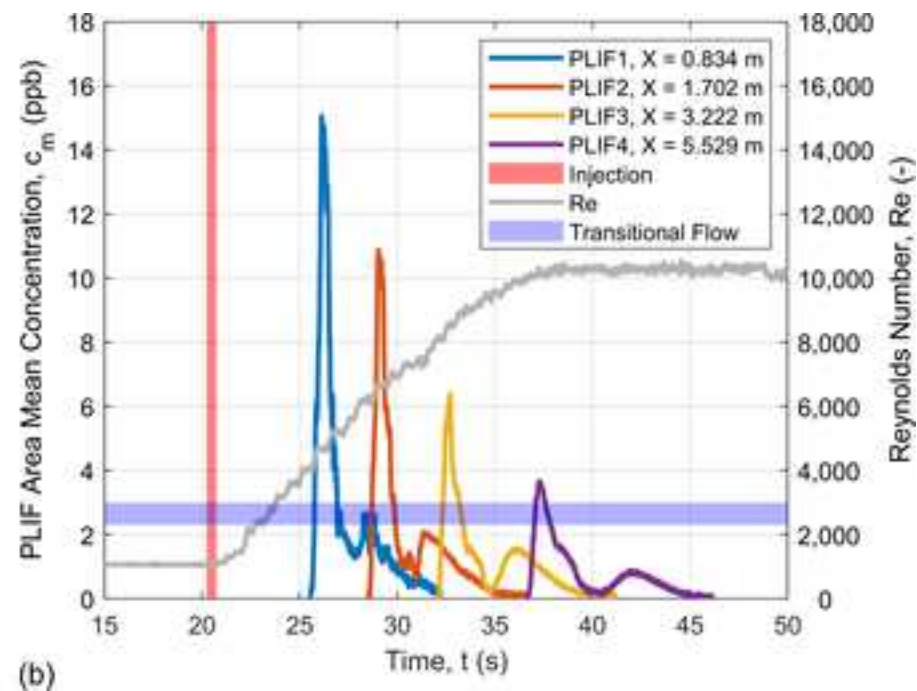








(a)



(b)

